

Elastic Bag Model for Molecular Dynamics Simulations of Solvated Systems: Application to Liquid Water and Solvated Peptides

Yuhui Li, Goran Krilov, and B. J. Berne*

Department of Chemistry, Columbia University, 3000 Broadway, New York, New York 10027

Received: December 27, 2005; In Final Form: April 18, 2006

The fluctuating elastic boundary (FEB) model for molecular dynamics has recently been developed and validated through simulations of liquid argon. In the FEB model, a flexible boundary which consists of particles connected by springs is used to confine the solvated system, thereby eliminating the need for periodic boundary conditions. In this study, we extend this model to the simulation of bulk water and solvated alanine dipeptide. Both the confining potential and boundary particle interaction functions are modified to preserve the structural integrity of the boundary and prevent the leakage of the solute–solvent system through the boundary. A broad spectrum of structural and dynamic properties of liquid water are computed and compared with those obtained from conventional periodic boundary condition simulations. The applicability of the model to biomolecular simulations is investigated through the analysis of conformational population distribution of solvated alanine dipeptide. In most cases we find remarkable agreement between the two simulation approaches.

I. Introduction

Molecular dynamics simulations have emerged as a powerful tool complementing experimental techniques in the study of biomolecular processes. The latter invariably occur within the confines of the physiological solution. The solvent often plays a critical role in modulating the conformational energetics and dynamics of proteins, which allows them to perform their biological function. Accurate treatment of solvation is therefore crucial to the success of biomolecular simulations.

To treat the solvation effects correctly, one must include a large number (typically thousands) of solvent molecules in addition to the protein in the simulation system. The computational complexity associated with the large size of these systems limits the time scale of simulations to nanoseconds. On the other hand, biological processes involving conformational changes in proteins often occur on much longer time scales, ranging from microseconds to seconds. Since the majority of computational effort is spent on simulating the solvent, the detailed dynamics of which is usually of little interest, significant effort has been expended in devising more efficient means of treating solvation effects.

A well-established approach to this problem is to approximate the expensive sums over solvent configurations by an effective reaction field acting on the biomolecular solute. A number of “implicit solvent” models have been developed along these lines,^{1–7} the most widely used being the dielectric continuum approximations including the generalized Born model³ and the Poisson–Boltzmann equation (PB).⁵ Although numerous studies have been carried out using these models, it is still uncertain whether they can correctly capture the energetics of biomolecular processes.^{8–13}

Recently, a number of hybrid methods that combine explicit and implicit treatment of solvation have been introduced with a goal of improving the accuracy of solvation models. Early approaches based on statistical mechanical liquid state theories include the MTGLE method of Berkowitz et al.,^{14–16} the work of Berkowitz and McCammon based on Langevin dynamics,¹⁷

the mean field force approximation (MFFA) of Brooks and Karplus,^{18,19} and RISM-HNC integral equation treatment of Pettitt and Karplus.²⁰ More recent approaches which attempt to incorporate electrostatic polarization effects include the surface constrained all atom solvent model of King and Warshel^{21,22} and the reaction field with exclusion of Rullman and van Duijnen.²³ Beglov and Roux developed the spherical solvent boundary potential²⁴ which allowed for the volume fluctuations in the explicit regions and extended it to include a finite difference Poisson–Boltzmann treatment of electrostatics.²⁵ The model was implemented in several biomolecular simulation studies, including the electron transfer in proteins,^{26,27} solvation,^{28,29} and thermal stability of biomolecules,^{30–32} and the folding kinetics of proteins.^{33–35} Nonetheless, these approaches restrict the shape of the boundary to simple geometries for which analytic solutions for the electrostatic polarization are available.

Several of the newest models strive to alleviate this restriction. Beglov and Roux’s primary hydration shell³⁶ method uses a sum over spheres approach to characterize a nonspherical inner region, albeit lacking the reaction field treatment for electrostatics. The shell approximation for protein hydration model of Lüdemann and Wade³⁷ and the surface of active polarons method of Kimura et al.³⁸ attempt to model the electrostatic polarization through the use of surface charges and dipoles.

We have recently introduced a new solvent boundary model, the fluctuating elastic boundary (FEB), that is both suitable for molecular dynamics simulations and removes some of the above restrictions.³⁹ In this approach the explicit solvent region is surrounded by an elastic boundary that evolves dynamically to accommodate the shape fluctuations of the solute–solvent system inside. In addition to lower computational cost, this implementation provides several advantages: Since the boundary is expressed in terms of standard pairwise interactions, the model is easily incorporated into existing biomolecular force fields with little or no modification. The model is fully conservative and evolves via Hamiltonian dynamics. The model provides flexibility to tune both dynamic response of the boundary as well as static (tension) properties. The contributions

of the bulk solvent outside of the boundary can then be included via a dielectric continuum model. In this paper we extend the methodology to simulations of aqueous solutions of peptides. The paper is organized as follows. In section II we present the overview of the FEB model. In section III we use the method to compute structural and thermodynamics properties of liquid water. In section IV, we demonstrate the applicability of the method to biomolecular simulations by computing the free energy landscape of alanine dipeptide in an aqueous solution. We conclude in section V.

II. Method

A. Fluctuating Elastic Boundary Model of Liquid Water.

In a previous paper, we introduced the fluctuating elastic boundary (FEB) model and applied it to the simulation of liquid argon. Both the structural and dynamic properties of liquid argon calculated from the FEB model are in excellent agreement with the results of the conventional molecular dynamics (MD) simulation. In the FEB model, the elastic boundary is modeled as a network of quasi-particles, which are connected with their nearest neighbors by elastic bonds. The resulting macromolecular arrangement has a topology of a spherical cage (similar to fullerenes). The boundary confines the solute–solvent system inside through a short-range repulsive interaction. In our previous work³⁹ we showed how the FEB model can be successfully implemented to study nonpolar systems. However, in most cases of biological interest, one has to deal with polar solvents. To investigate the application of the FEB model to such a system, we chose liquid water as a test case due to its importance as the primary biological solvent and the availability of structural and dynamic data.

The functional form of the bond potential was chosen empirically not only to provide flexibility to the boundary network but also to maintain sufficient stiffness to prevent leakage of the solvent molecules through the boundary. Hence, in this implementation we use a polynomial interaction

$$U_b(r_{ij}) = \begin{cases} ar_{ij}^6 & r_{ij} \leq r_0 \\ ar_{ij}^6 + b(r_{ij} - r_0)^{36} & r_{ij} > r_0 \end{cases} \quad (1)$$

where a and b are constants governing the stiffness of the bond, r_{ij} is the distance between two bonded boundary particles, and r_0 is reference distance. For liquid water at room temperature, we find that when setting a to be small ($\sim 10^{-8}$ kcal/mol·Å⁶), the first term supplies an adequate weak binding potential between boundary quasi-particles, while the second term restrains the distance between quasi-particles to be smaller than $\sim (r_0 + 1 \text{ \AA})$ with b also set to be small. r_0 is chosen as large as possible but still small enough to prevent the leakage of the solvent through the boundary. We found that the value of $2.5\sigma_b$, where σ_b is the range of the boundary–solvent repulsion, works well. When $r_{ij} > (r_0 + 1 \text{ \AA})$, the bond between the quasi-particles i and j becomes sufficiently stiff that the probability that a large hole might form on the boundary is very small. The confining potential is provided through a pairwise interaction of each of the boundary particles with the atoms of solute–solvent system inside. The interaction form is taken to be the repulsive Lennard-Jones (LJ) potential of the Weeks–Chandler–Andersen (WCA) form⁴⁰ as in our previous paper.³⁹ The number of boundary particles should be kept small for computational efficiency but large enough to allow sufficient boundary flexibility and avoid excessive pressure on the system inside due to boundary surface strain. We find that choosing a number of particles such that the mean distance between nearest

neighbors is comparable to the enclosed solvent diameter leads to good results.

The fluctuating boundary was constructed from 240 quasi-particles arranged in the spherical geometry and connected by a network of 360 bonds. We employ the simple point charge (SPC) water model developed by Berendsen et al.,⁴¹ which is an effective pair potential. The representative configuration of 200 SPC water molecules enclosed by the boundary (subsequently referred to as the “solute”) was initially selected from a conventional molecular dynamics simulation of 512 water molecules with periodic boundary conditions. For simplicity, the LJ parameters of the WCA potential were chosen to be the same as the oxygen LJ parameters of the SPC model. This is also consistent with the view of our system as comprising a cluster of water molecules dissolved in identically interacting liquid water.

To compute the contribution to the electrostatic interactions from the bulk solvent region outside the boundary, we have initially implemented a Poisson–Boltzmann (PB) model based on the DelPhi program,⁷ which is one of the fastest and most robust PB solvers available. The boundary surface separating the low-dielectric solute region from the high dielectric solvent required by this model is defined as the solvent accessible surface traced out by a spherical probe moving outside the boundary. For water, the appropriate radius of the probe is 1.4 Å. The internal and the external dielectric constants are set as 1 and 65, respectively, which is consistent with the SPC model of water. However, there are some disadvantages to this choice: (i) Finite grid sizes used by DelPhi to solve the PB equation lead to systematic errors in electrostatic potentials, particularly in the region close to the dielectric boundary. As a result, the total energy is not conserved but rather increases or decreases monotonically with time. Hence, we cannot compare the energy of water molecules in the FEB model with that in the conventional periodic boundary condition simulation. (ii) Since SPC water molecules will have lower electrostatic energy in regions of higher dielectric constant, they tend to migrate out of the boundary. Thus the probability of water molecules escaping outside the boundary is great. (iii) Although more accurate algorithms to solve the PB equation exist, such as the method by Im et al.,⁴² the computational effort required at each time step leads to very time-consuming simulations.

Our preliminary simulation studies both with and without the PB continuum model showed that the differences in computed structural properties of water are minimal (results not reported). Hence, we chose not to include the PB continuum in the simulations reported in this work. In addition to avoiding the difficulties described above, this approach allows us to qualify the degree to which long-range electrostatic interactions (beyond the first few solvation shells) influence the local structure and dynamics of the solvent. The electrostatic potential between water molecules inside the boundary was computed through direct computation of pairwise Coulomb interactions.

In parallel, the bulk system of 256 SPC water molecules was simulated under the conventional cubic periodic boundary condition. The density of the bulk was adjusted to match that observed in the FEB model. The static and dynamic properties of liquid water simulated using our model were then compared with those obtained from the PBC simulations. The results are reported in the following section.

B. Fluctuating Elastic Boundary Model of Alanine Dipeptide.

We next applied the FEB model to a prototypical biomolecular problem, namely, computing the thermodynamic properties of solvated alanine dipeptide (ADP). The peptide is

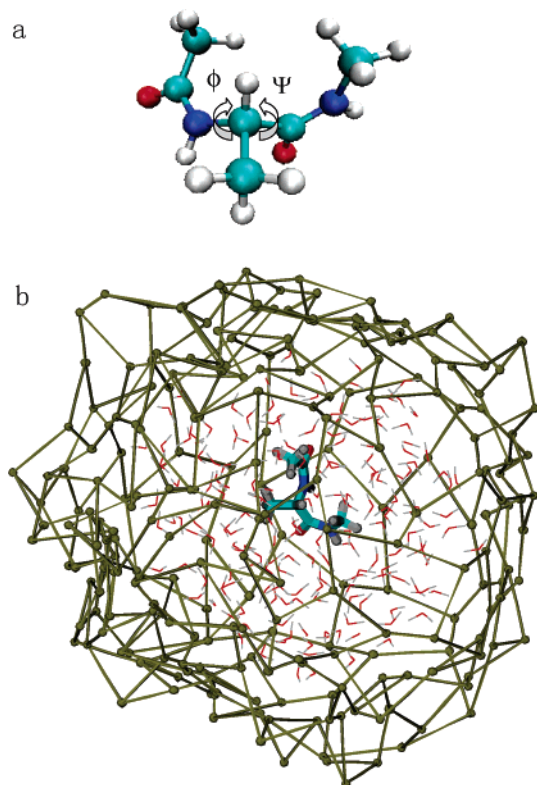


Figure 1. The fluctuating elastic boundary model of solvated alanine dipeptide. (a) The alanine dipeptide molecule with the dihedral angles ψ and ϕ indicated by arrows. (b) The ADP molecule in a cluster of water surrounded by the FEB mesh (tan).

composed of the NAC-ALA-ACE sequence, with 22 atoms. This system is often studied as it exhibits many properties characteristic of a larger polypeptide chain. Most notably, the conformational space of ADP is well characterized by the dihedral angles ψ and ϕ , shown in Figure 1a, which describe the rotation around the C $_{\alpha}$ -C and C $_{\alpha}$ -N bonds, respectively, in the same manner as the corresponding angles of protein backbone chains.

The FEB was implemented as a mesh of 240 quasi-particles connected by nearest neighbor bonds, with interactions as described in the previous section. Figure 1b illustrates the solvated ADP molecule enclosed by the FEB. OPLSAA 2001 force field⁴³ was used to describe all ADP interactions, and geometric combining rules were used for water-peptide LJ interactions. In addition to the WCA interaction, a harmonic interaction of the form

$$V(r) = \sum_j \epsilon_{\alpha}(r_{\alpha j} - R_b)^2 \quad (2)$$

was included between the C $_{\alpha}$ of the ALA residue of ADP and the boundary quasiparticles in order to keep the peptide fully solvated near the center of the cluster. R_b was chosen to be the average distance of the COM of the water cluster from the boundary surface, as estimated from the water cluster simulations, and $r_{\alpha j}$ is the distance between C $_{\alpha}$ and the j th boundary particle. Without the former potential, ADP was found to drift toward the surface of the cluster and in some instances escape through the boundary during the simulation.

For comparison we have also performed reference calculations on ADP solvated in SPC water using periodic boundary conditions and standard OPLSAA 2001 force field, at a solvent density comparable to that observed in the FEB model of liquid water.

III. Simulation of Liquid Water

We performed the FEB simulation of SPC water according to the following scheme. The mass of the boundary particles was set as $m_b = 50$ au and the bond constants and the reference distance are chosen as $a = 10^{-8}$ kcal/mol $\cdot\text{\AA}$,⁶ $b = 10^{-9}$ kcal/mol $\cdot\text{\AA}$,³⁶ and $r_0 = 3.5$ \AA . These parameters allow sufficient flexibility of the boundary, while keeping the SPC water molecules contained throughout the simulation. While all Coulomb interactions between water molecules were computed explicitly, a smooth cutoff was imposed on the LJ interaction at $r_c = 10$ \AA . All the simulations were performed using the SIM MD package⁴⁴ developed in our group. In FEB method, the system was first equilibrated through a canonical simulation at a temperature of 298 K. The structural and dynamic properties of the FEB model of liquid water were computed from five microcanonical trajectories for the standard FEB application. Each of the trajectories was 500 ps long generated with the time step 1 fs. The configurations were saved every 0.02 ps. The density of liquid water in the first method was observed to be approximately $\rho = 1.04$ g/cm³.

A. Structural Properties. 1. Pair Correlation Function.

The principal goal of the FEB method is to allow accurate simulation of localized processes in solvated systems. Hence we restricted our analysis of structural and dynamics properties to molecules close to the center of mass of the solvated cluster and sufficiently distant from the boundary.

We calculated the localized oxygen-oxygen, oxygen-hydrogen, and hydrogen-hydrogen pair correlation functions according to

$$g_{AB}(r) = \frac{1}{\rho} \frac{1}{N_c} \sum_{i|r_i < R_c} \langle \sum_{j \neq i} \delta(\mathbf{r} - \mathbf{r}_{i_A/B}) \rangle \quad (3)$$

by considering the correlation of a subset of N_c water molecules within a sphere radius $R_c = 5.0$ \AA centered at the center of mass (COM) of the water cluster. This is in contrast with the conventional molecular dynamics simulation with periodic boundary conditions, where all molecules contribute equally to the pair correlation function. The results for $g_{AB}(r)$ are shown in Figure 2. The pair correlation functions obtained from the FEB model simulation are shown in comparison with the result obtained from a simulation of bulk water with periodic boundary conditions at the density $\rho = 1.04$ g/cm³.

For the O-O pair correlation function, the main features are the first sharp peak and the second broader peak centered at 2.8 and 4.5 \AA , respectively. Figure 2a clearly shows these two features. We can see that the FEB model simulation result is in excellent agreement with the result obtained from the PBC molecular dynamics simulations in terms of both peak positions and heights in the range $r < 6.0$ \AA . The first minimum in $g_{OO}(r)$ from the PBC model is a little deeper than the corresponding result of the FEB model. Figure 2b displays the O-H pair correlation functions from the FEB model and PBC model. The two agree with each other very well for $r < 5.5$ \AA . The two sharp peaks near ~ 1.8 \AA and ~ 3.3 \AA are both well reproduced, except for the slight height differential in the second peak. The H-H pair correlation functions given in Figure 2c also show a high degree of overlap in the range $r < 5.0$ \AA , which includes the principal peaks at 2.4 and 3.9 \AA . For larger distances, $g_{AB}(r)$ of the FEB models are lower than those of the PBC results. This effect is expected and is due to the finite size of our system, which leads to a drop-off of the density as we approach the boundary of the solvated cluster, with $g(r) \rightarrow 0$ as $r \rightarrow R_{\text{boundary}}$.

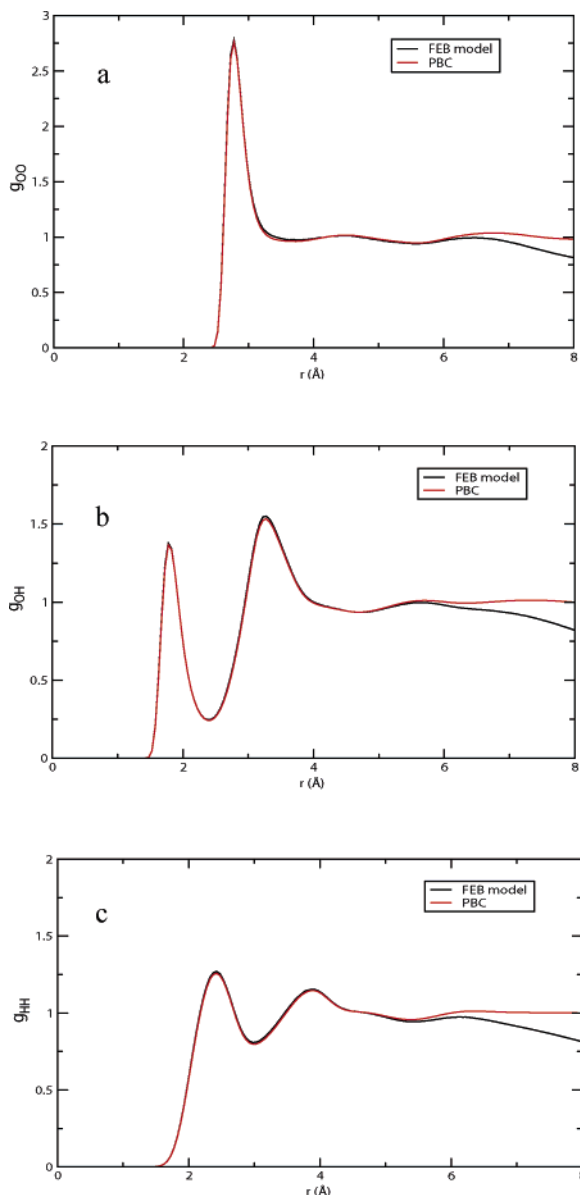


Figure 2. The O–O, O–H, and H–H pair correlation functions for the SPC liquid water model. The red line shows the PBC simulation results, and the black line shows the FEB simulation results.

TABLE 1: The Kinetic Energy and the Potential Energy (in kcal/mol) of the Water Molecules in the FEB Model and Conventional PBC Simulation^a

	kinetic energy	LJ potential energy	Coulomb energy
FEB model	0.883	1.835	-11.853
PBC model	0.889 ± 0.019	1.802 ± 0.022	-11.813 ± 0.093

^a The values for the FEB models were computed for the particles in the core region, and the agreement with PBC results is excellent. The density of the PBC simulation is $\rho = 1.04 \text{ g/cm}^3$.

2. Kinetic and Potential Energy. In Table 1 we compare the average per-particle kinetic, LJ, and electrostatic potential energy of water molecules in the FEB model with those computed from a molecular dynamics simulation using PBC. The kinetic energy was computed for the N_c water molecules contained in the sphere of radius $R_c = 5.0 \text{ \AA}$ centered at the COM of the water cluster according to

$$\langle T \rangle = \left\langle \frac{1}{N_c} \sum_{i|r_i < R_c} \frac{1}{2} m v^2 \right\rangle \quad (4)$$

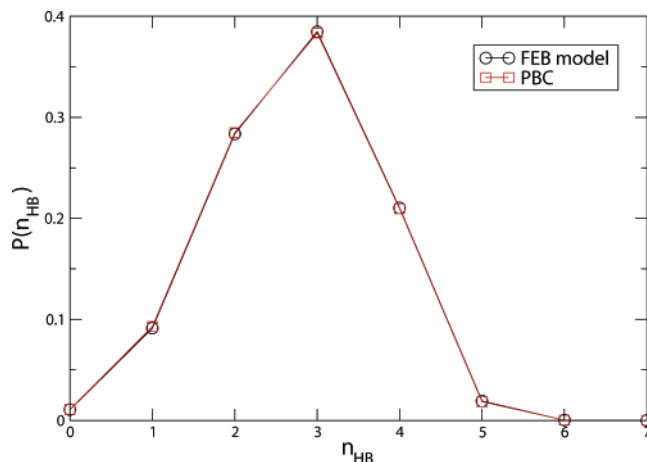


Figure 3. The distribution of the number of hydrogen bonds in liquid water, computed from the FEB model simulations (black line) and the PBC simulations (red line).

The average per-particle kinetic energy obtained from the FEB model is somewhat lower than that in the conventional simulation due to slight difference in effective temperatures, caused by the removal of COM motion for the water cluster.

The LJ potential energy was likewise computed according to

$$\langle U \rangle = \left\langle \frac{1}{2N_c} \sum_{i|r_i < R_c} U_{LJ}(r_{ij}) \right\rangle \quad (5)$$

by averaging all pair interactions of N_c molecules contained in the core region and all water molecules within the range of interaction. In the above equation, $r_{ij} = |\mathbf{r}_i - \mathbf{r}_j|$ and U_{LJ} is the standard LJ potential for $r_{ij} < r_c$ where the $r_c = 10 \text{ \AA}$. The values of the average per-particle LJ potential energy are close to each other for the two models. The LJ potential energy is slightly higher in the FEB model, which is consistent with the lower water density in the region $r_{ij} > 6 \text{ \AA}$ observed in the O–O pair correlation data. The electrostatic energy for the FEB model was calculated by direct evaluation of the Coulomb pair interactions in the same fashion as the LJ potential energy, while we used the particle–particle particle–mesh (P³M) algorithm for the PBC model. The values of the average electrostatic energy are nearly identical. Hence, we can conclude that the FEB model correctly describes the solvent polarization in the core region. We should point out that the electrostatic energy is easier to compute in the FEB method, due to a reduced number of pair interactions that need to be evaluated. Overall, both kinetic and potential energies are in excellent agreement with the PBC result.

3. Hydrogen Bond Distribution. Hydrogen bonds (HBs) play a significant role in both the structural properties and the dynamic behavior of liquid water. We employed the geometric definition of the water–water hydrogen bond, which implies that a water pair is hydrogen bonded if the oxygen–oxygen distance is no greater than 3.5 \AA and, simultaneously, the O–H···O angle is no less than 150° . For the FEB model, we only considered the water molecules in the core region described previously. In other words, at least one of the two molecules which constitute the hydrogen bond must be located in the core region. The distribution of hydrogen bond counts per water molecules was computed and is shown in Figure 3. The peaks of both distribution curves coincide at $n_{HB} = 3$. The two curves nearly overlap one another, which illustrates that the two models have very similar local structure of hydrogen bonds. We

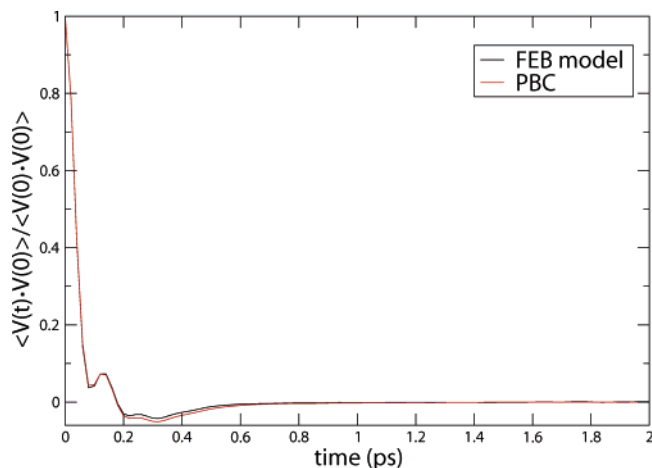


Figure 4. The molecular velocity autocorrelation function for liquid water. The black line gives the FEB simulation results, while the red line gives the PBC simulation results.

conclude that, at least in the core region, the FEB model mimics the local hydrogen bond environment with accuracy comparable to that of a conventional PBC simulation.

B. Dynamic Properties. 1. Velocity Autocorrelation Function. The normalized velocity autocorrelation function provides a sensitive characterization of the dynamics of the system and allows the evaluation of the self-diffusion coefficient via the Green–Kubo relation (eq 7). The velocity autocorrelation function is computed according to

$$C_{vv}(t) = [N_c \langle v^2 \rangle]^{-1} \sum_{i|r_i(0) < R_c} \langle \mathbf{v}_i(0) \cdot \mathbf{v}_i(t) \rangle \quad (6)$$

with only the trajectories initiating in the core region ($r_i(0) < R_c = 5.0 \text{ \AA}$) contributing to the ensemble average. Figure 4 shows the velocity autocorrelation functions computed from the PBC and the FEB model molecular dynamics simulations. The results for both models are in very good agreement. At long times the C_{vv} computed via the FEB model is well behaved with a smooth decay to zero in ~ 0.6 ps, which is much shorter than the mean time for the particle to diffuse into the boundary region. This allows the self-diffusion coefficient to be estimated from the velocity autocorrelation data using the finite-time approximation to the Green–Kubo relation

$$D = \frac{1}{3} \int_0^T \langle \mathbf{v}(0) \cdot \mathbf{v}(t) \rangle dt \quad (7)$$

with $T \gg 0.6$ ps, and $T \ll \infty$, even though the infinite time limit of the above integral would necessarily yield $D = 0$, due to the confined nature of our system. In our previous paper³⁹ we determined D using an alternate approach, based on the decay of autocorrelation functions of an eigenfunction of the diffusion operator subject to spherical boundary conditions. This approach was first introduced by Liu et al.⁴⁷ in their study of diffusion near liquid–vapor interfaces. This method gave values for D equal to that which we find using the above procedure. The integrals were evaluated numerically for the two functions up to $t = 3$ ps. The diffusion coefficient computed from the FEB model is $0.421 \pm 0.036 \text{ \AA}^2/\text{ps}$, slightly higher than $0.368 \pm 0.037 \text{ \AA}^2/\text{ps}$ obtained using PBC.

2. Dynamics of Hydrogen Bonds. The dynamics of water–water hydrogen bonds is of significant importance in characterization of the dynamic properties of biomolecules in aqueous solution. We investigated the dynamics of hydrogen bonds by two methods: through the hydrogen bond autocorrelation

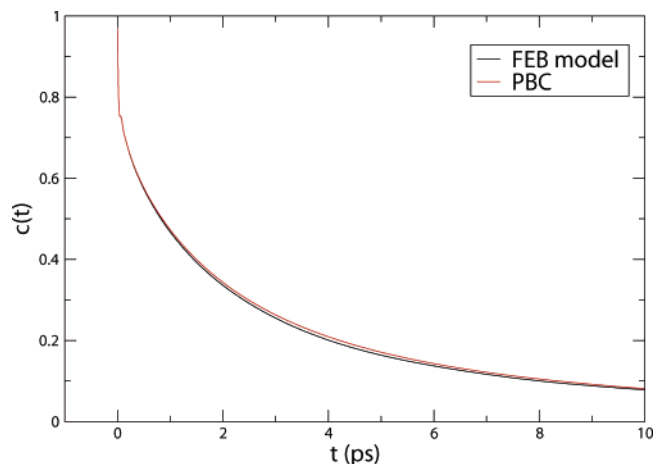


Figure 5. The hydrogen bond autocorrelation function for liquid water, computed from FEB (black line) and PBC (red line) simulations.

function (HBAF) $c(t)$ and via the conditional time-dependent probability of breaking hydrogen bonds (CTDPBHB) $O(t)$. Both of these were used by Xu and Berne to study the hydrogen bond kinetics in the solvation shell of a polypeptide.⁴⁵ The two HB autocorrelation functions were evaluated for the water molecules in the core region as described previously. The HBAF characterizes the structural relaxation of hydrogen bonds and is defined as

$$c(t) = \langle h(0)h(t) \rangle / \langle h \rangle \quad (8)$$

where $h(t) = 1$ if the tagged water pair is hydrogen bonded at time t and $h(t) = 0$ otherwise. $c(t)$ is the probability that a hydrogen-bonded water pair at time $t = 0$ is still hydrogen bonded at time t . The $c(t)$ computed using the FEB model and PBC simulation data is shown in Figure 5. The short time decays exhibited by both models are in excellent agreement. It is well-known that the kinetics of hydrogen bonds for times longer than 1 ps is related to translational pair diffusion of water.⁴⁶ To remove the contributions from pair diffusion, the second function CTDPBHB was calculated

$$O(t) = \langle h(0)(1 - h(t))H(t) \rangle / \langle h(0)H(t) \rangle \quad (9)$$

where $H(t) = 1$ if the tagged water pair is closer than 3.5 \AA at time t and $H(t) = 0$ otherwise. $O(t)$ is the conditional probability that a hydrogen bond is broken at time t but the involved pair of water molecules are still close to each other. Thus, this approach allows us to obtain detailed information about the dynamics of HB, while excluding the effect of the diffusion of water molecules. The $O(t)$ values computed from the FEB simulations and the PBC simulations are shown in Figure 6. The two functions agree with each other for time $t < 5$ ps, while at longer times $O(t)$ from the PBC simulation attains higher values than the FEB simulation result. For $t > 5$ ps some tagged water molecules diffuse out of the core and enter a region where boundary effects are more pronounced. This causes $O(t)$ of the FEB model to plateau at a lower value than that of the PBC model, implying that water molecules remain hydrogen bonded for a longer time out of the core region. The latter observation is consistent with the concerted mechanism for hydrogen bond dynamics: A hydrogen bond will break only if the participating molecule is able to form new hydrogen bonds with neighboring molecules. Since there is a pronounced deficit of hydrogen bonding capable molecules in the vicinity of the boundary, the opportunity to find another hydrogen bonding partner is significantly diminished. This effect was first observed by Liu

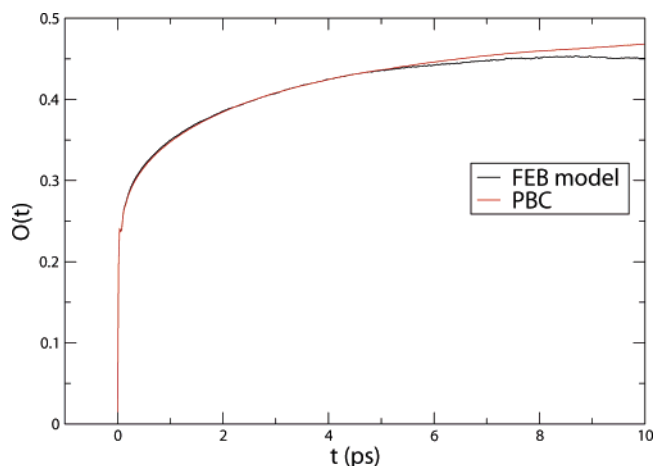


Figure 6. The conditional time-dependent probability of breaking hydrogen bonds for liquid water, computed from FEB (black line) and PBC (red line) simulations.

et al.⁴⁷ in their study of hydrogen bond dynamics near air–water interfaces.

IV. Simulation of Alanine Dipeptide

The alanine dipeptide (ADP) molecule was built using the Meastro program (Schrodinger). The geometry was first optimized by energy minimization in a vacuum. OPLSAA 2001 parameters were used to describe all bonded and nonbonded interactions. A cluster of 200 SPC water molecules enclosed by the FEB consisting of 240 quasi-particles was prepared as in section II.A, and equilibrated at 300 K for 100 ps. Constant temperature was maintained through the use of Nose-Hoover thermostats.⁴⁸ All FEB model simulations were performed using the SIM package. The FEB potential parameters (boundary particle mass, bond constants and WCA parameters) were identical to the ones given in the previous section. All LJ interactions were truncated smoothly at $r_c = 10 \text{ \AA}$, while no cutoff was imposed on the Coulomb interactions. The ADP was then placed in the center of the water cluster, and 22 overlapping molecules were removed. The resulting system consisting of a single ADP molecule solvated by 178 SPC molecules and enclosed by the FEB was equilibrated for an additional 200 ps. Five 1000 ps trajectories were then computed using initial configurations selected randomly from the last 50 ps of the equilibration run, and the time step of 1 fs. The configurations were saved every 0.02 ps.

In parallel, we performed a simulation of ADP solvated in SPC water using the standard PBC approach. A box of SPC water was equilibrated, and the box size was adjusted to obtain a density of $\rho = 1.0395 \text{ g/cm}^3$, consistent with that observed in FEB model simulations. An ADP molecule was placed in the center of the box and the overlapping water molecules were removed, and a 100 step steepest descent minimization was used to remove steric clashes between the waters and the peptide. This resulted in a system of 670 water molecules solvating the ADP in a box of length $L = 27.0 \text{ \AA}$. OPLSAA force field parameters were used for all bonded ADP interactions, and geometric combining rules were used for water–peptide LJ interactions. Particle–mesh Ewald (PME) was used to treat long-range electrostatics, while smooth switch/shift cutoffs at $R_c = 12.0 \text{ \AA}$ were imposed on all short-range Coulomb and LJ terms. The system was then equilibrated for 5000 ps with 1 fs time step. Constant temperature of 298 K was maintained through the use of Nose-Hoover thermostats. Ten configurations were saved at 100 ps intervals from the last 1000 ps of the

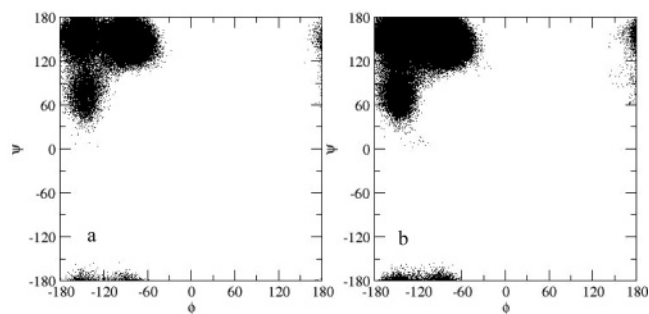


Figure 7. The Ramachandran plots for alanine dipeptide dihedral angle distributions from (a) FEB model simulations and (b) PBC simulations. The FEB data are based in 250000 conformations, while the PBC data contain 50000 conformations.

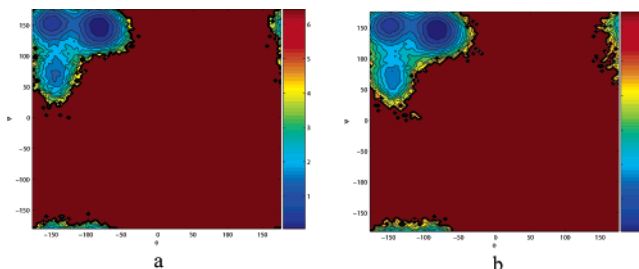


Figure 8. The relative free energy maps for alanine dipeptide as a function of the dihedral angles (ϕ, ψ) from (a) FEB model simulations and (b) PBC simulations. The FEB data are based in 250000 conformations, while the PBC data contain 50000 conformations.

equilibration run and used to initiate production runs. The production run consisted of 10 trajectories, each of 10000 ps. The configurations were saved every 2 ps, which yielded a total of 50000 configurations collected over a combined 100 ns simulations. The long intervals were chosen to ensure adequate sampling of the relevant regions of ADP conformational space.

A. Conformational Analysis. The data from both FEB and PBC simulations were then used to construct ϕ – ψ Ramachandran maps for ADP, which are shown in Figure 7. The maps are in excellent agreement with each other indicating that both models produce a very similar equilibrium distribution of ADP conformations. Most of the configurations are clustered in the upper left region of the (ϕ, ψ) plane, which is consistent with experimental observations of highly populated extended states in the β -strand region of the Ramachandran diagram. The data were then histogrammed into 4° bins and the resulting population distribution used to compute the relative free energy of ADP as a function of the two dihedral angles according to

$$\Delta G = -k_B T \ln \left[\frac{P(\phi, \psi)}{P_{\max}} \right] \quad (10)$$

where k_B is the Boltzmann constant, $P(\phi, \psi)$ is the population distribution function, and P_{\max} is the maximum population observed. Figure 8 shows the contour plots of the relative free energy landscape for the FEB model and PBC simulation. In both cases there are three free energy basins with significant populations corresponding to stable states: The proline-like P_{II} state centered at $(-80, 145)$, is the most stable, followed by a somewhat less populated extended C_5 located at $(-150, 150)$, and a shallow minimum in the β region centered around $(-150, 70)$. These results are consistent with recent two-dimensional infrared (2D-IR) and NMR measurements on small peptides,⁴⁹ which conclusively show that the P_{II} state is the most populated one, while separate polarized-Raman FTIR measurements point

TABLE 2: Comparison of the Locations of Principal Free Energy Minima of Solvated Alanine Dipeptide and the Relative Populations of Each of the Three Stable States, Obtained from the FEB Model and the Conventional PBC Simulations

	ϕ	ψ	rel free energy	percentage, %
PBC minimum 1	-82 ± 14	150 ± 14	0.0	33.3
FEB minimum 1	-82 ± 14	150 ± 14	0.0	34.6
PBC minimum 2	-150 ± 10	154 ± 10	0.43	9.4
FEB minimum 2	-150 ± 10	154 ± 10	0.46	9.1
PBC minimum 3	-142 ± 10	70 ± 18	1.61	2.4
FEB minimum 3	-142 ± 10	70 ± 18	1.65	2.0

TABLE 3: Comparison of Computational Efficiencies of the FEB and PBC Models

case	CPU time per time step
FEB simulation	0.057
PBC simulation	0.340

to an existence of a stable extended state.^{50,51} Moreover, the free energy profiles for the FEB model are in excellent agreement with those computed by PBC. Table 2 shows the positions and relative free energies of the three minima for both models, as well as the relative populations of each state. Once again, the two agree remarkably well, demonstrating that the FEB approach accurately models the thermodynamics of ADP.

We should point out that we had not observed any significant population in the α_R conformation, located around $(-80, -60)$. Several studies based on different force field–water model combinations predict a varying degree of population in this state,⁴⁹ and there is experimental evidence of a small amount of helical conformations for alanine tripeptide.⁵² We did observe a shallow minimum in the α_R region for a PBC simulation of our OPLSAA/SPC model at a lower density $\rho = 1.00 \text{ g/cm}^3$. We believe the shift in the water structure around ADP at higher densities slightly destabilizes this state. In any case, this effect is not important for the purpose of the validation of the FEB model.

B. Computational Efficiency. Finally, we used the alanine dipeptide study to investigate the computational efficiency of our FEB approach for the simulation of solvated biomolecules. This is important, as improving the computational efficiency is a primary driver for the development of hybrid solvation models. The systems considered were of comparable size, with 475 water molecules solvating ADP in the PBC simulation, and 178 water molecules and 240 boundary particles surrounding ADP in the FEB simulations, and the time steps used in each case were identical. In Table 3 we compare the CPU time expended per time step of the FEB and PBC simulations, respectively. According to this measure, and in the current implementation, the FEB simulations are nearly five times more efficient than the corresponding PBC results. This is primarily due to the costly sums over periodic images that must be performed in the latter, to correctly account for the effects of long-range electrostatic forces. We should point out that the inclusion of a continuum dielectric model in the FEB approach would somewhat reduce its computational advantage. However, it is plausible that in that case, one would be able to reduce the number of explicit molecules enclosed by the boundary while still retaining the accurate treatment of solvation. Hence, while current performance results are very encouraging, improving the FEB model to strike an optimal balance between computational expediency and accurate treatment of the solvent effects remains a goal of future work.

V. Conclusions

In this paper we have extended the fluctuating elastic boundary model introduced previously to allow simulations of liquid water, the most important biological solvent, as well as solvated biomolecules. We have found that even for moderately sized water clusters of 200 molecules, the FEB simulations accurately reproduce the local structure and energetics, including the hydrogen bonding network. The dynamic properties of water are likewise in very good agreement with the results of conventional molecular dynamics simulation. The FEB model leads to water dynamics that is slightly faster than that predicted by PBC simulations, as well as slightly longer hydrogen bond lifetimes. We believe these are the consequences of the interruption of the hydrogen bonding network in the immediate vicinity of the boundary, which relieves the frictional drag and increases diffusivity in the outermost layers of the confined droplet. Such an effect was observed before by Lee and Rossky⁵⁴ in their study of structure and dynamics of liquid water near hydrophobic and hydrophilic surfaces: The diffusion in the vicinity of a hydrophobic surface was considerably enhanced compared to that near a hydrogen-bonding hydrophilic surface. This can be corrected by adding an appropriately directional anisotropic term to the boundary–water interaction potential, which would restore correct orientational ordering of outer layer water molecules consistent with the bulk liquid hydrogen bond network structure. Nonetheless, even without these corrections, the dynamic properties considered are in agreement within the statistical error.

We note that the average density of water in the FEB model calculations presented in this paper is approximately 4% higher than that of liquid water at room temperature and atmospheric pressure. This has been observed in other hybrid solvation model studies as well^{53,24} and is almost certainly due to boundary effects. For example, it is well-known that water clusters exhibit nonuniform density profiles, with density in their centers being higher than that of the bulk liquid. Our simulations of water droplets with no boundary potentials indicate densities up to 10% higher than the bulk in core regions. In this case, the boundary force is provided only by the surface tension of the cluster. We are currently exploring several approaches to alleviating this problem, such as the modification of the boundary potential to include the attractive component of the dispersion potential and the increase in the number of boundary particles in order to relieve surface strain.

As the goal of the FEB approach is to develop a model for efficient and accurate treatment of solvation in biomolecular simulations, we further validated the former by performing flexible boundary simulations of solvated alanine dipeptide, along with accompanying reference PBC simulations. The canonical configurational population distribution for alanine dipeptide is adequately characterized by the distribution of the two backbone dihedral angles, and hence the Ramachandran plots and the related (ϕ, ψ) free energy landscapes provide an accurate measure of the ability of the FEB simulations to produce the correct equilibrium distributions. The overall agreement between the free energy surfaces computed from FEB and PBC simulations is very good, including both the relative energies, locations, and population distribution among the three stable states. This is particularly encouraging as it is well-known that the free energy landscapes of small peptides are very sensitive to the solvation effects, with different solvation models sometimes producing qualitatively different results.^{9,10} One current limitation of our model is the limited ability to control the solvent density within, which complicates comparison with

PBC results. Further improvements in the solute–boundary interaction potential in combination with a more realistic treatment of long-range electrostatics are likely to alleviate this problem and will be the subjects of future research.

Acknowledgment. This work was supported by a grant to B.J.B. from NSF (CHE-03-16896).

References and Notes

- (1) Roux, B.; Simonson, T. *Biophys. Chem.* **1999**, *78*, 1.
- (2) Born, M. Z. *Phys.* **1920**, *1*, 45.
- (3) Still, W. C.; Tempczyk, A.; Hawley, R. C.; Hendrickson, T. *J. Am. Chem. Soc.* **1990**, *112*, 6127.
- (4) Warshel, A.; Levitt, M. *J. Mol. Biol.* **1976**, *103*, 757.
- (5) Nicholls, A.; Honig, B. *J. Comput. Chem.* **1991**, *12*, 435.
- (6) Gilson, M. K.; Davis, M. E.; Luty, B. A.; McCammon, J. A. *J. Phys. Chem.* **1993**, *97*, 3591.
- (7) Honig, B.; Nicholls, A. *Science* **1995**, *268*, 1144.
- (8) Zhou, R.; Berne, B. J.; Germain, R. *Proc. Natl. Acad. Sci. U.S.A.* **2001**, *98*, 14931.
- (9) Zhou, R.; Berne, B. J. *Proc. Natl. Acad. Sci. U.S.A.* **2002**, *99*, 12777.
- (10) Zhou, R.; Krilov, G.; Berne, B. J. *J. Phys. Chem. B* **2004**, *108*, 7528.
- (11) Bursulaya, B. D.; Brooks, C. L., III. *J. Phys. Chem. B* **2000**, *104*, 12378.
- (12) Calimet, N.; Shaefer, M.; Simonson, T. *Proteins: Struct., Funct., Genet.* **2001**, *45*, 144.
- (13) Mezei, M.; Fleming, P. J.; Srinivasan, R.; Rose, G. D. *Proteins: Struct., Funct., Biol.* **2004**, *55*, 502.
- (14) Berkowitz, M.; Brooks, C. L., III; Adelman, S. A. *J. Chem. Phys.* **1980**, *72*, 3889.
- (15) Brooks, C. L., III; Berkowitz, M.; Adelman, S. A. *J. Chem. Phys.* **1980**, *73*, 4353.
- (16) Adelman, S. A.; Brooks, C. L., III. *J. Phys. Chem.* **1982**, *86*, 1511.
- (17) Berkowitz, M.; McCammon, J. A. *Chem. Phys. Lett.* **1982**, *90*, 215.
- (18) Brooks, C. L., III; Karplus, M. *J. Chem. Phys.* **1983**, *79*, 6312.
- (19) Brunger, A.; Brooks, C. L., III; Karplus, M. *Chem. Phys. Lett.* **1984**, *105*, 495.
- (20) Pettitt, B.; Karplus, M. *Chem. Phys. Lett.* **1987**, *136*, 383.
- (21) Warshel, A.; King, G. *Chem. Phys. Lett.* **1985**, *121*, 124.
- (22) King, G.; Warshel, A. *J. Chem. Phys.* **1989**, *91*, 3647.
- (23) Rullman, J. A.; van Duijnen, P. T. *Mol. Phys.* **1987**, *61*, 293.
- (24) Beglov, D.; Roux, B. *J. Chem. Phys.* **1994**, *100*, 9050.
- (25) Im, W.; Bernèche, S.; Roux, B. *J. Chem. Phys.* **2001**, *114*, 2924.
- (26) Basu, G.; Kitao, A.; Kuki, A.; Go, N. *J. Phys. Chem. B* **1998**, *102*, 2076.
- (27) Basu, G.; Kitao, A.; Kuki, A.; Go, N. *J. Phys. Chem. B* **1998**, *102*, 2085.
- (28) Roux, B. *Biophys. J.* **1996**, *71*, 2076.
- (29) Nina, M.; Beglov, D.; Roux, B. *J. Phys. Chem. B* **1997**, *101*, 5239.
- (30) Sugita, Y.; Kitao, A. *Proteins* **1988**, *30*, 388.
- (31) Sugita, Y.; Kitao, A. *Biophys. J.* **1988**, *75*, 2178.
- (32) Sugita, Y.; Kitao, A.; Go, N. *Folding Des.* **1988**, *27*, 173.
- (33) Marchand, S.; Roux, B. *Proteins* **1988**, *33*, 265.
- (34) Mohanty, D.; Elber, R.; Thirumalai, D.; Beglov, D.; Roux, B. *J. Mol. Biol.* **1997**, *272*, 423.
- (35) Kitao, A.; Hayward, S.; Go, N. *Proteins* **1988**, *33*, 496.
- (36) Beglov, A.; Roux, B. *Biopolymers* **1995**, *35*, 171.
- (37) Lounnas, V.; Lüdemann, S. K.; Wade, R. C. *Biophys. Chem.* **1999**, *78*, 157.
- (38) Kimura, S. R.; Brower, R. C.; Zhang, C.; Sugimori, M. *J. Chem. Phys.* **2000**, *112*, 7723.
- (39) Li, Y.; Krilov, G.; Berne, B. J. *J. Phys. Chem. B* **2005**, *109*, 463.
- (40) Chandler, D.; Weeks, J. D.; Andersen, H. C. *Science* **1983**, *220*, 787.
- (41) Berendsen, H. J. C.; Postma, J. P. M.; van Gunsteren, W.; Hermans, J. *Intermolecular Forces*; Pullman, B., Ed.; Reidel: Dordrecht, The Netherlands, 1981.
- (42) Im, W.; Beglov, D.; Roux, B. *Comput. Phys. Commun.* **1998**, *111*, 59.
- (43) Jorgensen, W. L.; Maxwell, D. S.; Tirado-Rives, J. *J. Am. Chem. Soc.* **1996**, *118*, 11225.
- (44) Stern, H.; Xu, H.; Harder, E.; Rittner, F.; Pavese, M.; Berne, B. J. **2000**.
- (45) Xu, H.; Berne, B. J. *J. Phys. Chem. B* **2001**, *105*, 11929.
- (46) Luzar, A.; Chandler, D. *Nature* **1996**, *379*, 55.
- (47) Liu, P.; Harder, E.; Berne, B. J. *J. Phys. Chem. B* **2005**, *109*, 2949.
- (48) Martyna, G. J.; Klein, M. L.; Tuckerman, M. *J. Chem. Phys.* **1992**, *94*, 2365.
- (49) Mu, Y.; Kosov, D. S.; Stock, G. *J. Phys. Chem. B* **2003**, *107*, 5064.
- (50) Schweitzer-Stenner, R.; Eker, F.; Huang, Q.; Griebenow, K. *J. Am. Chem. Soc.* **2001**, *123*, 9628.
- (51) Eker, F.; Cao, X.; Nafie, L.; Schweitzer-Stenner, R. *J. Am. Chem. Soc.* **2001**, *123*, 9628.
- (52) Woutersen, S.; Mu, Y.; Stock, G.; Hamm, P. *Proc. Natl. Acad. Sci. U.S.A.* **2001**, *98*, 11254.
- (53) Lee, M. S.; Salsbury, F. R., Jr.; Olson, M. A. *J. Comput. Chem.* **2004**, *25*, 1967.
- (54) Lee, S. H.; Rossky, P. J. *J. Chem. Phys.* **1994**, *100*, 3334.